Plant Root-Inspired Soil Penetration in Sands Using Circumnutations for Geotechnical Site Characterization

Riya Anilkumar,¹ Yuyan Chen, PhD^{2,3} and Alejandro Martinez, PhD⁴

¹Department of Civil and Environmental Engineering, University of California Davis, Davis, CA 95616; E-mail: ranilkumar@ucdavis.edu

²Department of Civil and Environmental Engineering, University of California Davis, Davis, CA 95616; E-mail: yychen@ucdavis.edu

³National Facility for Earthquake Engineering Simulation, Tianjin University, Tianjin 300350, China

⁴Department of Civil and Environmental Engineering, University of California Davis, Davis, CA 95616; E-mail: amart@ucdavis.edu

ABSTRACT

Subsurface exploration is vital for characterizing the soil engineering properties at project sites. Current in-situ testing methods often face challenges providing necessary reaction forces in sites with limited accessibility or with stiff surficial layers (i.e. desiccated or gravelly crusts). This paper presents two investigations on the circumnutation-inspired penetration strategy to decrease the vertical penetration forces. Both investigations were performed on dry sands, one consisting of experimental tests using a robotic arm and the second involving Discrete Element Modeling (DEM) simulations. In plant-inspired circumnutative penetration, the penetrometer's tip follows a helical path. The bio-inspired probes used in this study have conical tips that are bent at an angle and the entire probes are rotated at different angular velocities while they are advanced into the soil at a vertical velocity. The cumulative total work required to push the probes (i.e. the sum of the rotational and vertical work) was calculated and compared with that involved in quasi-static penetration (i.e. in Cone Penetration Tests). Both the experimental and simulation results show a dependence of the vertical force and torque mobilized during penetration on the relative velocity of the probe tip, defined as the ratio of the tip's tangential to vertical velocities. Namely, the vertical penetration force decreases as the relative velocity is increased, leading to a decrease in vertical work. The torque remains relatively constant for the circumnutation tests, but the rotational work increases with relative velocity. The total work of circumnutative penetration is similar or slightly smaller than that required for quasi-static penetration for small magnitudes of relative velocities for both experimental investigations and simulations. These findings show that circumnutative penetration can mobilize significantly smaller lower penetration resistances than quasi-static penetration while requiring a similar or slightly smaller amount of work. The reduction in penetration force would allow smaller equipment to be used in site investigation soundings.

INTRODUCTION

Characterizing the soil engineering properties at project sites through subsurface exploration is vital before development. Current in-situ testing methods like the Cone Penetration Test (CPT) and the dilatometer test (DMT) often face challenges due to the insufficient reaction mass at sites

with limited accessibility or with stiff surficial layers (i.e. desiccated or gravelly crusts), leading to refusal. In these cases, the use of a more energy efficient penetration strategies would be beneficial. Efficient penetration strategies could also allow for installation of sensors to monitor conditions, such as piezometers or accelerometers, with lighter equipment. Apart from site investigation, more efficient penetration strategies would also be useful for applications of underground infrastructure development such as tunneling and deep foundation installation.

In addition to engineering, diverse organisms in nature such as plant roots, snakes, worms and clams employ various penetration strategies that have evolved over time to maximize energy efficiency (Martinez et al. 2022). By drawing inspiration from these natural adaptations, engineering strategies can be derived to create energy-efficient penetration methods. Recent developments in the field of bio-inspired geotechnics include the development of self-burrowing probes and robots (e.g., Huang & Tao 2020; Chen et al. 2021), tree-root inspired anchors and foundations (e.g., Burrall et al. 2020), and snakeskin-inspired surfaces and piles (e.g., Martinez et al. 2019; O'Hara and Martinez 2022).

This study draws inspiration from plant roots whose tip follow a helical trajectory while they penetrate the soil. This is known as circumnutation motion and is observed in a range of plant species (Taylor et al. 2021, Dottore et al. 2016). Figure 1 illustrates the circumnutation motion exhibited by a rice root. The tip of the root is bent at angle and the root rotates with an angular velocity while moving downward with a vertical velocity. In this study, the penetration performance and energy efficiency of a bio-inspired probe is evaluated in comparison to that of a non-rotating quasi-static penetration probe (i.e. CPT probe). An idealized schematic of a probe that uses circumnutation-inspired motion (CIM) is shown in Figure 1 (b). The bio-inspired probe has a tip bent at an angle (α) with a bent length of (L_I). The probe is rotated at an angular velocity (ω) while it is displaced with a vertical velocity (ν). The distance R depicted in the figure, which is the distance between the tip of the probe and the probe's central axis, is a function of the probe diameter (D), the tip's apex angle (δ), α , and L_I .

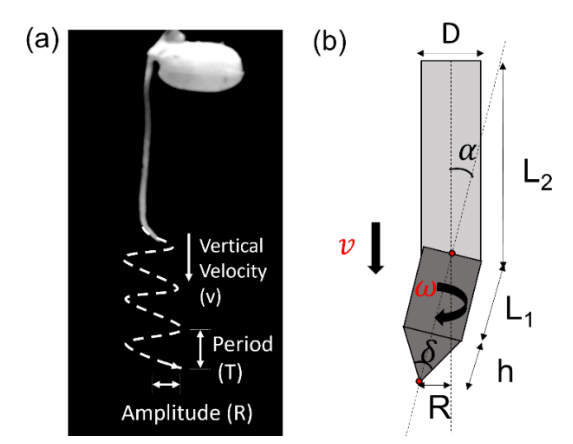


Figure 1: (a) Circumnutation motion of a rice root characterized by its period, vertical velocity, motion amplitude and tip geometry (after Taylor et al. 2021). (b) Schematic of probe that employs circumnutation-inspired motion.

This paper presents the results of two investigations, one experimental and one numerical. In both investigations, circumnutation-inspired motion (CIM) tests were performed using bio-inspired probes while the penetration forces and torques were recorded with depth. The vertical, rotational, and total work components were computed as a function of the relative velocity, defined

as the ratio of the tip's tangential velocity to its vertical velocity ($\omega R/\nu$). The results are compared to the penetration forces and work components of a CPT test with the same probe diameter and vertical velocity. It is noted that the numerical model is not calibrated against the experimental results; therefore the results should be considered as independent investigations.

METHODS

Experimental Setup. The CIM penetration experiments were performed in deposits of uniform dry sand models prepared at a target relative density of 40%. The sand deposits were prepared by raining sand from a fixed height (i.e. air pluviation). The sand referred to as "100A" in Ahmed et al. 2023 was used in this investigation. This quartz sand is poorly-graded and is composed of subangular particles. It has a median particle size (D_{50}) of 0.18 mm, 10^{th} percentile particle size (D_{10}) of 0.12 mm, coefficient of uniformity (C_U) of 1.74, coefficient of curvature (C_C) of 1.04, and critical state friction angle (φ'_{cs}) of 32.1°.

The experimental setup used a UR16e robotic arm (Universal Robots) to control the vertical displacement, a motor and gearbox to control the angular velocity, and a six-axis load cell to measure the forces and torques. During the CIM penetration, the probe penetrated to a depth of 15 cm at a v of 0.5 mm/s. For different penetration tests, ω was varied while keeping v constant to produce different relative velocities ranging from 0.25π to 4π . This range was chosen as different species of plants were found to have relative velocities of 0.2π to 1.6π during circumnutation (Chen and Martinez 2023). The non-rotating probe (NRP) test was conducted using a CPT probe while maintaining the same vertical velocity as the CIM tests. The vertical force (F_Z) and torque (T_Z) with is recorded with depth. An image of the setup is presented in Figure 2(a).

The idealized probe shown in Figure 1 (b) was used as a basis for the design of the experimental probe used in all the CIM tests. The bio-inspired probe was fabricated out of aluminum tubing with a D of 12.7 mm, δ of 60°, L_I of 12.7 mm (equivalent to D) and an α of 10°. Figure 2 (b) shows an image of the bio-inspired probe. A straight, non-rotational probe (NRP) with the same diameter and cone apex angle was also fabricated to perform CPT tests to provide a comparison against the CIM results.

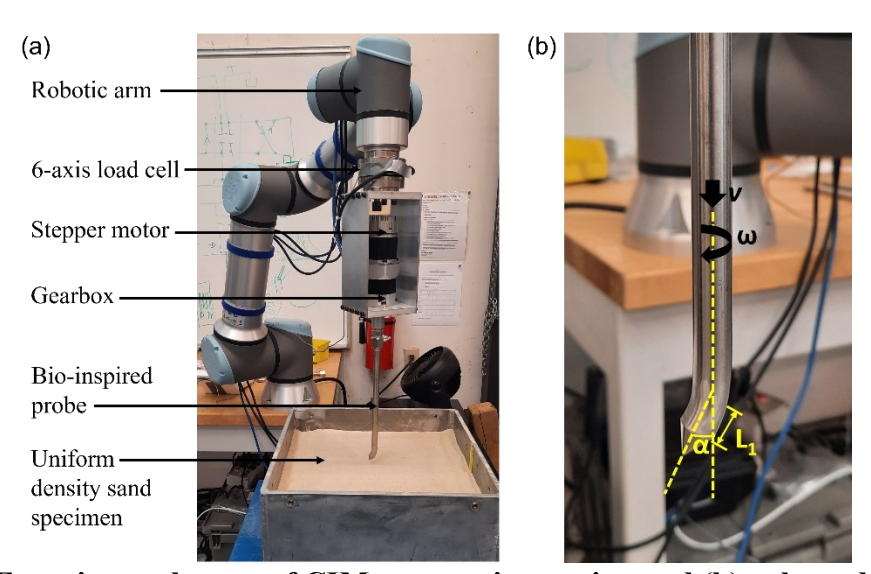


Figure 2: (a) Experimental setup of CIM penetration testing and (b) enlarged image of the bio-inspired probe.

DEM Model. The DEM simulations of the CIM penetration were performed using the PFC 3D (version 5.0, Itasca) software. The DEM model consists of a chamber, a bio-inspired probe and soil particles. The chamber has a diameter of 1.0 m and height of 0.7 m, constructed by a cylindrical and bottom wall (Figures 3(a) and (b)). The simulation parameters adopted have been previously shown by Chen et al. 2021 and 2022 to produce behaviors that are representative of natural sands. The particle contacts are modeled using a linear contact model with rolling resistance. The following parameters were used in the simulations: normal stiffness to particle diameter $(k_n/D) = 10^8 \text{ N/m}^2$, normal to shear stiffness ratio $(k_n/k_s)=1.5$, normal stiffness of probe $(k_{n,p})=1.4 \times 10^7 \text{ N/m}$, shear stiffness of probe $(k_{s,p})=9.5 \times 10^6 \text{ N/m}$, interparticle friction coefficient $(\mu_{pp})=0.4$, rolling coefficient $(\mu_{pp})=0.4$, particle-probe friction coefficient $(\mu_{pp})=0.3$, particle-wall friction coefficient $(\mu_{pw})=0$, and particle density $(\rho)=2650 \text{ kg/m}^3$. The DEM specimen consists of about 278,200 spherical particles. The specimen has a void ratio of 0.61.

The simulated bio-inspired probe has a diameter of 0.044 m (D) and an apex angle of 45°. The probe has a similar configuration as described for the experiments, with an inclined bottom shaft with length L_I of 0.044 m (i.e. $L_I = D$) and an inclined conical tip with an angle α of 10°. During the penetration process, the probe is rotated while it is displaced downward at a constant velocity. In contrast to the experiment, the top shaft (probe section in light gray in Figure 1(b)) is not rotated. In each simulation, the probe is displaced from the soil surface to a depth of 0.3 m.

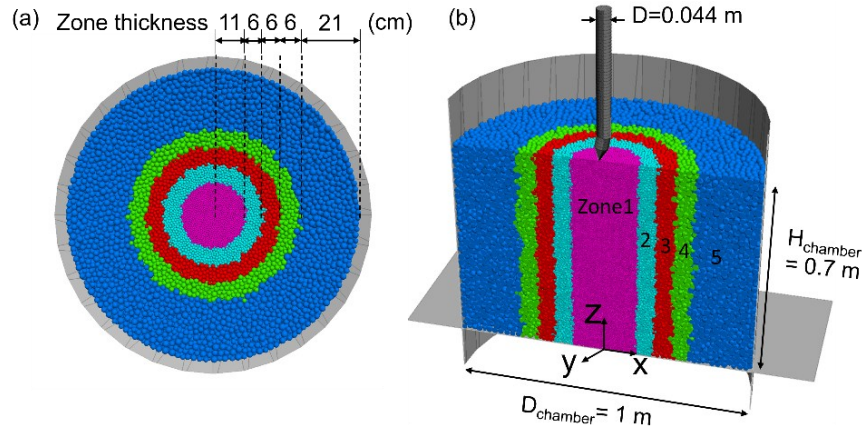


Figure 3: Specimen used for DEM CIM penetration simulations. (a) Plan and (b) side view.

The specimen is constructed using the particle refinement method.

The particle sizes were upscaled in relation to those of natural sand particles, which is a common strategy to reduce the computational expense of DEM simulations. This study employs the particle refinement method (PRM) to increase the number of probe-particle contacts by using small particle in the center zone (zone 1 in Figure 3), while also maintaining an affordable computational cost by increasing particle sizes towards the lateral boundary (McDowell et al. 2012). The specimen developed for this study has particles with D_{50} of 6.31 mm in the center zone, where the probe-particle contacts occur. The particle sizes increase gradually in the other four zones, with D_{50} of 9.47 mm, 14.20 mm, 17.04 mm and 20.45 mm in zones 2, 3, 4 and 5, respectively. The particle upscaling factors between the adjacent zones are 1.2 or 1.5 to prevent particle migration between different zones (McDowell et al. 2012). The soil in each zone is poorly graded with a C_U of 1.2 and a C_C of 0.96.

EXPERIMENTAL RESULTS

During the penetration tests, the vertical penetration force and torque along the probe's longitudinal axis were measured for the CIM and NRP test, and their variation with relative velocity was observed. The vertical work (W_V) was computed as the product of the vertical force and the vertical displacement, and the rotational work (W_R) was computed as the product of the torque and rotational displacement (Equation 1 and 2). The total work was calculated as the sum of the vertical and rotational work components (Equation 3).

$$W_V = \sum F_Z v \Delta t \tag{1}$$

$$W_R = \sum T_Z \omega \Delta t \tag{2}$$

$$W_T = W_V + W_R \tag{3}$$

Force, Torque and Mechanical Work. The vertical penetration forces mobilized during CIM decreased with an increase in $\omega R/v$, while the torque magnitudes were higher for the CIM tests than for the NRP case. Both the vertical forces and torques increase with depth. Figure 4 (a) and (b) illustrate the variation of vertical force and torque with depth for different $\omega R/v$ along with the NRP experiments. Increases in $\omega R/v$ led to an exponential reduction of the average vertical force. Figure 5(a) presents the F_Z measurements averaged between depths of 10 and 14 cm. At an $\omega R/v$ of 4 π , the F_Z magnitude is 3.9% of that mobilized in the NRP test, while at $\omega R/v$ of 0.5 π and 0.25 π the F_Z magnitudes are 35.0% and 45.3%, of that in NRP test, respectively. While there is no T_Z generated during the NRP test, significant T_Z magnitudes were mobilized during all the CIM cases. The results show small differences in the average torque magnitudes (between depths of 10-14 cm) for the different CIM tests (Figure 5(b)).

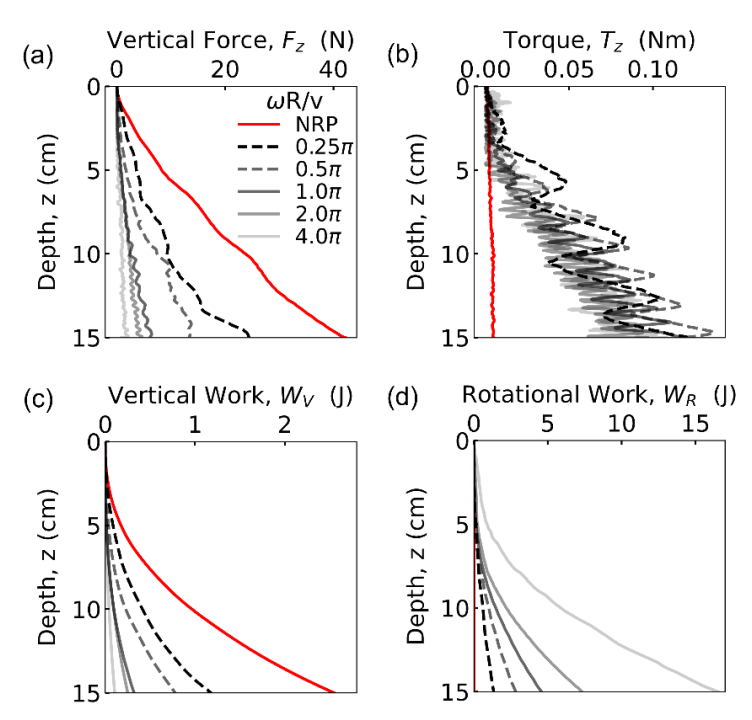


Figure 3: Experimental results indicating the variation of (a) vertical force (b) torque (c) vertical work and (d) rotational work with depth for different relative velocities.

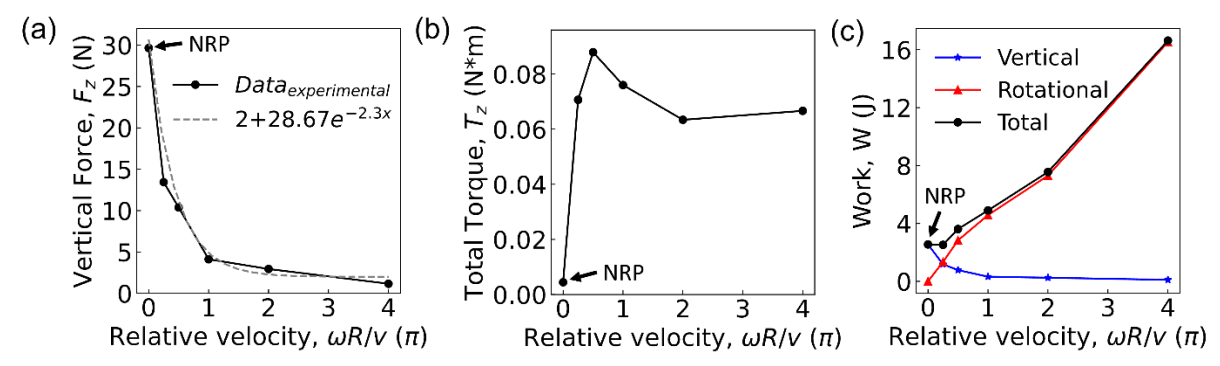


Figure 4: Experimental variation of (a) average vertical force, (b) average torque, and (c) work components with increasing relative velocity.

The vertical work is smaller for the CIM penetration tests, and its magnitude decreases with increasing $\omega R/v$, while the rotational work increases with $\omega R/v$. The variation of Wv and WR with depth for different $\omega R/v$ of CIM is depicted in Figure 4 (c) and (d), while Figure 5 (c) shows the cumulative Wv, WR and WT at the end of penetration (depth of 15 cm) as a function of with $\omega R/v$. The Wv exponentially decays with increasing $\omega R/v$, following the same trend as the FZ relationship since all the tests have same vertical displacement (i.e. $v\Delta t$). WR increases roughly linearly with increasing $\omega R/v$. While the TZ magnitude remains roughly constant for the CIM tests, the increase in WR is driven by the linear increase in rotational displacement (i.e. $\omega \Delta t$) with ω .

As a result of the variations in W_V and W_R , the W_T first slightly decreases and then increases as $\omega R/v$ is increased. The total work of circumnutative penetration is slightly lower (by 1%) than that of NRP for small values of $\omega R/v$ but is higher than that for NRP with further increase in $\omega R/v$. Based on interpolation of the data, $\omega R/v$ ranging from 0 π to 0.26 π yield similar W_T than NRP. The maximum reduction in F_Z in this range of $\omega R/v$ is 51%.

DEM SIMULATION RESULTS

During CIM, the total vertical force, total torque, and mechanical work components are recorded considering the contributions from all probe sections (i.e., the top shaft, bottom shaft, and tip). The F_Z magnitude is calculated as follows:

$$F_Z = \sum_{i=1}^{N_1} F_{Ztip,i} + \sum_{j=1}^{N_2} F_{Zshaft1,j} + \sum_{k=1}^{N_3} F_{Zshaft2,k}$$
 (4)

where $F_{Ztip,i}$ is the vertical component of contact force i acting on the probe tip, $F_{Zshaft1,j}$ and $F_{Zshaft2,k}$ are the vertical components of the contact force j and k acting on the bottom and top shafts, respectively, and N_1 , N_2 and N_3 are the total number of vertical component forces on the tip, bottom shaft and top shaft, respectively.

Since the top shaft does not rotate, the T_Z is the sum of torque components acting on the tip and bottom shaft as defined in Eq. 5:

$$T_{Z} = \sum_{i=1}^{N_{1}} (F_{Xtip,i} d_{Xtip,i} + F_{Ytip,i} d_{Ytip,i}) + \sum_{j=1}^{N_{2}} (F_{Xshaft1,j} d_{Xshaft1,j} + F_{Yshaft1,j} d_{Yshaft1,j})$$
(5)

where $F_{Xtip,i}$ and $F_{Ytip,i}$ are the two i^{th} horizontal component forces acting on the tip, $d_{Xtip,i}$ and $d_{Ytip,i}$ are the distances at which the i^{th} horizontal component forces act with respect to the axis of

rotation (i.e. probe centerline), $F_{Xshaft1,j}$ and $F_{Yshaft1,j}$ are the horizontal component forces acting on the bottom shaft, and $d_{Xshaft1,j}$ and $d_{Yshaft1,j}$ are the corresponding distances from the axis of rotation. The total work, vertical, and rotational work are computed as defined in the previous section using equation (1) (2) and (3).

Force, Torque and Mechanical Work. The CIM simulations with different $\omega R/\nu$ ranging from 0.25 π to 4 π are examined to understand the effects on the total F_Z , total T_Z and work. CIM penetration leads to a large reduction in the tip resistance with increasing $\omega R/\nu$ compared to that measured during NRP (Figure 6(a)). The torque during CIM penetration is greater than during NRP, with small differences in T_Z between the simulations with varying relative velocities (Figure 6(b)). These F_Z and T_Z trends agree with the experimental results (i.e., Figures 4 and 5). It is noted that in the simulation results shown in Figure 6(b) variation of T_Z around zero for the NRP case is caused by horizontal forces acting against the probe at any time that result in small but measurable torques. The average F_Z and T_Z values obtained during the last 0.05 m of penetration for different $\omega R/\nu$ are presented in Figures 7(a) and 7(b), respectively. As shown, the F_Z decreases exponentially with an increase in the relative velocity at a similar rate as the experimental results, with the 0.25 π , 0.5 π and 4 π cases mobilizing F_Z magnitudes equivalent to 53.0%, 32.0% and 11.3% of the F_Z for the NRP case, respectively (Figure 7(a)).

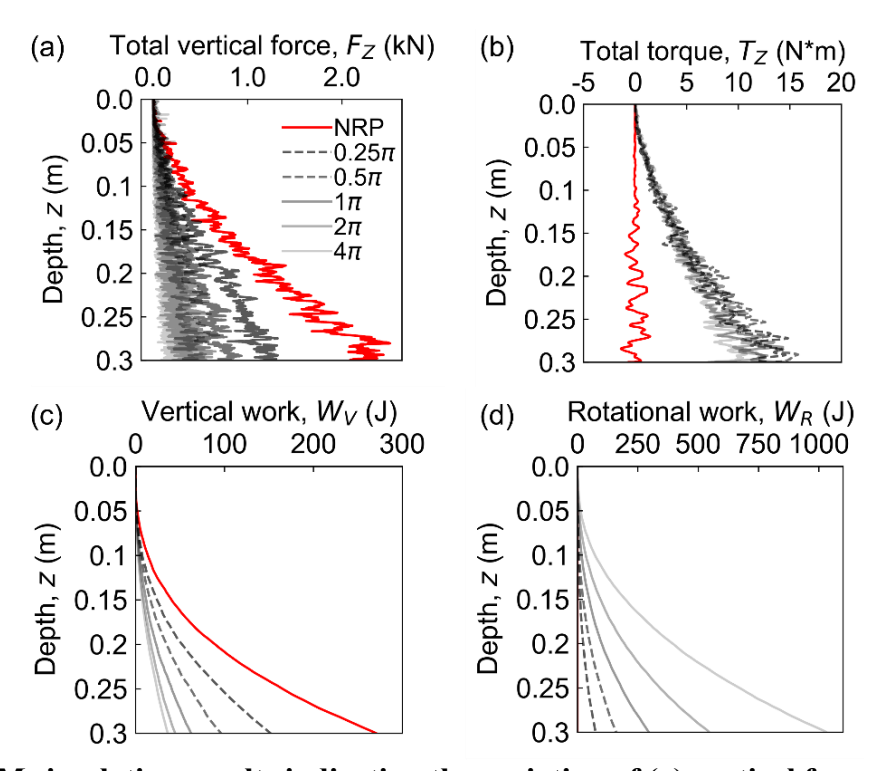


Figure 5: DEM simulation results indicating the variation of (a) vertical force (b) torque (c) vertical work and (d) rotational work with depth for different relative velocities.

Increasing the $\omega R/v$ leads to a decrease in the W_V and an increase in the W_R (Figures 6(c) and 6(d)). These trends are again consistent with the experimental results. The cumulative vertical, rotational and total work at the end of penetration are presented in Figure 7(c), showing the decrease in W_V and increase in W_R as the $\omega R/v$ is increased. The results show a decrease in the

total work from $\omega R/v$ from 0π to 0.25π , with a minimum value 16.2% smaller than the W_T for NRP. Similar to the experimental results, there is a range of $\omega R/v$ for which similar/lower W_T than NRP is required. Based on interpolation of the data, this range of $\omega R/v$ is from 0π to 0.55π which is higher than the range observed through experimental investigation. These differences are due to higher magnitudes of rotational work in comparison to vertical work for the experiments. This may be the result of the rotation of the entire probe (top and bottom shaft) in the experiments unlike just the rotation of the bottom shaft in the DEM simulations. The maximum reduction of penetration resistance at $\omega R/v$ for which similar/lower W_T than NRP is used is 31.1%.

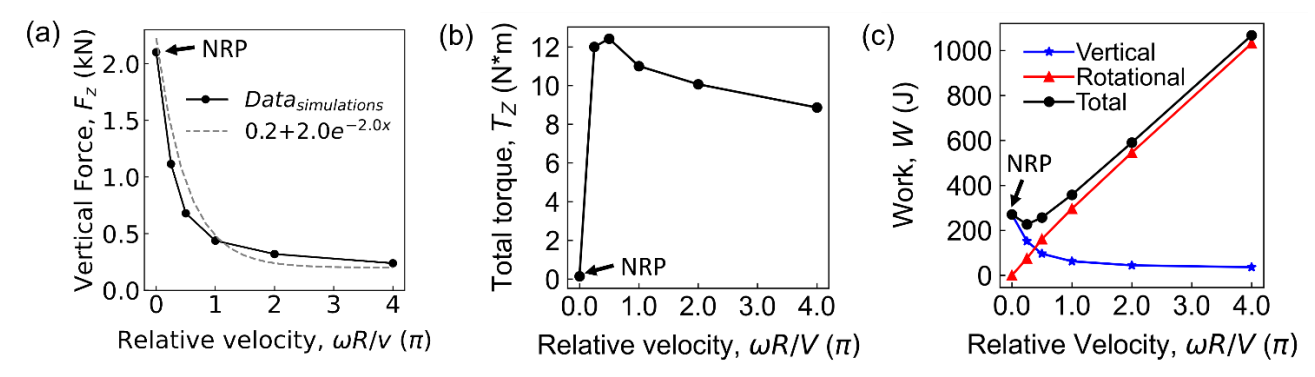


Figure 6: DEM variation of (a) average vertical force, (b) average torque, and (c) work components with increasing relative velocity.

Force Chains and Particle Displacements. The results of the NRP and two CIM simulations with relative velocities of 0.25π and 2π are analyzed in this section to examine the interactions between the probe and particles from a particle-level perspective. Figures 8 (a)-(c) presents spatial maps of total particle displacement magnitudes at the end of penetration (i.e. probe depth of 0.3 m) along a vertical cross-section through the center of the specimen. In these figures, the color of the particles is proportional to their displacement magnitude. The large displacements for the NRP case occur near the specimen surface where a conical wedge characteristic of a shallow failure is formed as well as along the probe's surface at greater depths. The size of the surficial wedge decreases as the $\omega R/v$ is increased for the CIM simulations, and at greater depths the zones with large particle displacements are sinuous which follow the tip's trajectory. The sinuous disturbed zone in the CIM simulation with 0.25π relative velocity is sparser than that in the 2π simulation, since there are only 2.4 revolutions during penetration for the former compared to 19.2 revolutions in the latter.

The contact force chains also show differences in the probe-particles interactions due to changes in the relative velocity. Figures 8(d)-(f) depict the normal contact forces greater than 5 N in force chain maps, where the thickness and color of the lines is proportional to the contact force magnitude between two particles or between a particle and the probe. Greater contact forces are located around the probe tip for the NRP simulation than for CIM cases, and the force magnitude decreases between the 0.25π and 2π cases. These observations are consistent with the reduction in F_Z as the relative velocity is increased (i.e. Figures 5(a) and 7(a)). The microscale results indicate that CIM facilitates penetration by altering the shape of the failure zone and changing the distribution and magnitude of contact forces around the probe, resulting in the reduction of vertical penetration forces compared to those in the NRP case.

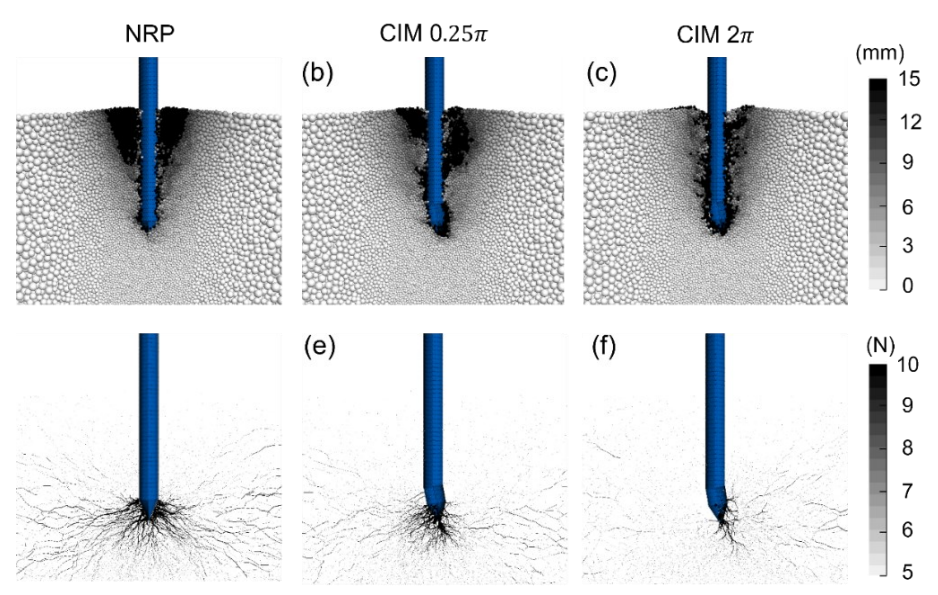


Figure 7: Particle displacement fields and force chains surrounding the probes for the (a) NRP, (b) CIM 0.25 π , and (c) CIM 2 π simulations.

CONCLUSIONS

Penetration experiments and DEM simulations of plant-root inspired probes that employ circumnutation-inspired motion were performed in this study. Circumnutation-inspired motion consist of a combination of rotational and vertically penetration motions on a probe with a bent tip. These experiments and simulations were performed on dry sands models with a uniform density. For this study, the probe geometry, sand density and vertical penetration velocity were maintained constant for all the tests. Non-rotational penetration tests were performed with a CPT probe with the same diameter and tip apex angle as the probe used for CIM tests. For the CIM tests, the angular velocity was varied which resulted in different relative velocities. The vertical force and torque magnitudes generated during penetration were recorded in both experiments and simulations, which were used to compute the vertical and rotational work components. The total work for penetration was defined as the sum of the vertical and rotational work.

Both the experimental and DEM simulations showed a dependence of the vertical forces and torques generated during penetration on the relative velocity. The vertical forces decayed exponentially with an increase in relative velocity. This decrease resulted in vertical forces generated during the CIM test at a relative velocity of 4 π of 3.9% and 11.3% of those generated in the experimental and numerical NRP tests, respectively. NRP penetration led to negligible mobilized torque while the CIM tests recorded similar torques magnitudes for different angular velocities. Particle-level analysis of the DEM results sheds light on the reasons for the decrease in vertical penetration force. The results show that that the volume of disturbed soil and the magnitude of contact forces around the probes decrease as the relative velocity is increased.

The cumulative total work done during CIM penetration was slightly smaller or similar in magnitude than that during NRP at $\omega R/v$ smaller than 0.26 π for the experiments and smaller than 0.55 π for the DEM simulations. At the range of $\omega R/v$ that led to smaller or similar total work, CIM penetration mobilized up to 51% and 31% smaller penetration forces than those mobilized during NRP for experimental and DEM investigation respectively. Since the vertical penetration force was found to exponentially decay with $\omega R/v$, this resulted in a concomitant decrease of

cumulative vertical work. The linear increase in angular displacement with increases in $\omega R/v$ resulted in an increase in rotational work.

Overall, the results indicate that CIM can be an equally or slightly more energy efficient penetration strategy while mobilizing lower vertical penetration forces if appropriate relative velocities are used. This could be further useful to minimize the power or energy use, and thus costs, for penetration to a certain depth in applications of subsurface exploration such as in-situ testing or placement of sensors. The significantly lower vertical resistance mobilized during CIM could also facilitate the use of smaller penetration equipment as lower vertical reaction forces would be necessary.

REFERENCES

- Ahmed, S. S., Martinez, A., & DeJong, J. T. (2023). Effect of gradation on the strength and stress-dilation behavior of coarse-grained soils in drained and undrained triaxial compression. *Journal of Geotechnical and Geoenvironmental Engineering*, 149(5).
- Burrall, M., DeJong, J. T., Martinez, A., & Wilson, D. W. (2020). Vertical pullout tests of orchard trees for bio-inspired engineering of anchorage and foundation systems. *Bioinspiration & Biomimetics*, 16(1).
- Chen, Y., Khosravi, A., Martinez, A., & DeJong, J. (2021). Modeling the self-penetration process of a bio-inspired probe in granular soils. *Bioinspiration & Biomimetics*, 16(4).
- Chen, Y., Martinez, A. & DeJong, J. (2022). Alteration of the stress state around a bio–inspired probe enables self–penetration. *Canadian Geotechnical Journal*, 59(10).
- Chen, Y. & Martinez, A. (2023). DEM modeling of root circumnutation-inspired penetration in shallow granular materials. Under review for possible publication in *Geotechnique*.
- Del Dottore, E., Mondini, A., Sadeghi, A., Mattoli, V., & Mazzolai, B. (2016, May). Circumnutations as a penetration strategy in a plant-root-inspired robot. In 2016 IEEE international conference on robotics and automation (ICRA) (pp. 4722-4728). IEEE.
- Huang, S., & Tao, J. (2020). Modeling clam-inspired burrowing in dry sand using cavity expansion theory and DEM. *Acta Geotechnica*, 15(8).
- Martinez, A., Dejong, J., et al. (2022). Bio-inspired geotechnical engineering: principles, current work, opportunities and challenges. *Géotechnique*, 72(8), 687-705.
- Martinez, A., Palumbo, S., & Todd, B. D. (2019). Bioinspiration for anisotropic load transfer at soil–structure interfaces. *Journal of Geotechnical and Geoenvironmental Engineering*, 145(10).
- McDowell, G. R., Falagush, O., & Yu, H. S. (2012). A particle refinement method for simulating DEM of cone penetration testing in granular materials. *Géotechnique Letters*, 2(3).
- O'Hara, K. B., & Martinez, A. (2020). Load transfer directionality of snakeskin-inspired piles during installation and pullout in sands. *Journal of Geotechnical and Geoenvironmental Engineering*, 148(12).
- Taylor, I., Lehner, K., McCaskey, E., Nirmal, N., Ozkan-Aydin, Y., Murray-Cooper, M., ... & Benfey, P. N. (2021). Mechanism and function of root circumnutation. *Proceedings of the National Academy of Sciences*, 118(8).